J. Fluid Mech. (2009), *vol.* 618, *pp.* 279–303.
doi:10.1017/S0022112008004643 Printed in the United Kingdom

Double-averaging analysis and local flow characterization of near-bed turbulence in gravel-bed channel flows

EMMANUEL MIGNOT†, E. BARTHELEMY AND D. HURTHER

Laboratoire des Ecoulements Géophysiques et Industriels (LEGI), BP 53, 38041 Grenoble Cedex 9, France

(Received 8 October 2007 and in revised form 15 October 2008)

This investigation focuses on the characteristics of near-bed turbulence in fully rough gravel-bed open-channel flows. The analysis combines results obtained with the double-averaging methodology and local flow characterization, using velocity measurements provided by a high-resolution three-axis Acoustic Doppler Velocity Profiler (ADVP). As a result of the flow heterogeneity induced by the bed topography, the flow is not locally uniform in the near-bed region, and a double-averaging methodology is applied over a length scale much greater than the gravel size. In smooth- and rough-bed flow conditions, without macro-roughness bed elements, maximum turbulent kinetic energy (TKE) production occurs very close to $z = 0$, while in our case with fully rough flows with macro-roughness elements, maximum turbulence activity is found to occur at gravel crest levels z_c ($z_c/h = 0.1$). Turbulent diffusion also reaches a maximum at this elevation. The characteristics of the spatially averaged TKE budget are in good agreement with those obtained in flows over canopies. The hydrodynamic double-averaged properties have strong similarities with mixing layers and reattached mixing layers in flows over backward facing steps. Local time-averaged velocity profiles can be split into three typical classes, namely log, S-shaped and accelerated. It appears that the S-shaped class profiles, located in the wakes of the macro-roughness elements, exhibit an inflectional profile typical of mixing layers. They are of major importance in the double-averaged TKE budget, as they provide a local high contribution to the double-averaged TKE flux, TKE production and dissipation compared to the log class profiles. Consequently, double-averaged TKE production is roughly 75 % greater than the dissipation rate at the point of maximal TKE production. Moreover the macro-roughness bed elements imply mixing-layer-type hydrodynamics that play a dominant role in the overall structure of mean near-bed turbulence of gravel-bed channel flows.

1. Introduction

The structure of turbulence in hydraulically rough open-channel flows has received much attention over the past decades (Chow 1959; Chaudry 1993; Nezu 1993; Nezu & Nakagawa 1993; Graf & Altinakar 1998). These pioneering studies provide useful information for engineering and research applications for which mean hydrodynamic

† Email address for correspondence: emmanuel.mignot@hmg.inpg.fr

quantities such as velocity profiles, turbulent shear, turbulent intensities, turbulent kinetic energy (TKE) production, dissipation and diffusion are necessary. Usually these studies assume locally two-dimensional mean flow conditions. Recently, several studies have shown that such an assumption is not valid for gravel-bed channel and river flows (Franca & Czernuszenko 2006; Franca & Lemmin 2006). In these conditions, the vertical distribution of mean flow quantities can vary significantly over a large part of the water column close to and within the bed roughness. Moreover, local properties of gravel-bed channel flows in the vicinity of the bed roughness are highly heterogeneous in space and therefore not representative of large-scale flow characteristics such as bottom drag which are often the only ones of use in engineering applications (Coleman *et al.* 2007). Moreover, a large amount of similar work has been produced in the field of atmospheric boundary layer flows (Britter & Hanna 2003; Coceal *et al.* 2006; Coceal, Dobre & Belcher 2007*a*; Coceal, Dobre & Thomas 2007*b*, *c*) and plant canopy interaction with wind (De Langres 2008) with, for the latter, special consideration for the dispersion of chemical substances.

Recently, double-averaging methods originally developed for atmospheric boundary layer studies (Wilson & Shaw 1977; Raupach & Shaw 1982) have been revisited in the framework of river hydraulics (Nikora *et al.* 2001; Aberle 2007; Coleman *et al.* 2007). One of these techniques was applied by Lopez & Garcia (2001) to study the structure of turbulence in an open-channel flow over a vegetation canopy. It consists of averaging the Navier–Stokes equations in time and space over an area contained in a plane parallel to the flow direction. This method takes into account the spatial heterogeneity in the mean flow quantities introduced by the bed geometry heterogeneity. Because double averaging (DA) can be applied from within the flow/bed interface and up to the free surface, it potentially offers new insights into macro-roughness element effects on mean benthic hydrodynamics, particularly when combined with local flow analysis. These new approaches should allow improvements in our understanding of coupled flow processes such as hyporheic flow exchange, sediment and pollutant transport and benthic bio-habitat dynamics.

However, sediment and vegetation canopies are in essence different with regard to how the density of the solid elements is vertically distributed, and the turbulence structure within the rough bed is therefore very different (Nikora *et al.* 2001). For instance Nikora *et al.* (2001, 2004) applied the double-averaging method to large, organized roughness element (so-called spherical-segment-type) bed flows and showed that the intrinsic averaged streamwise velocity profile is linear inside the bed roughness for hydraulically rough flows with high submergence while inflectional within vegetation canopies and urban canopies (Coceal *et al.* 2006, 2007*c*). They also showed that the shear stress variation is linear above the crest of the roughness elements, reaching a maximum at the crest level.

DA equations have been derived in recent years for the mass, momentum and energy budgets, but their application remains severely limited due the lack of measuring tools able to provide accurate flow measurements with sufficient spatio-temporal resolution above and within the flow/bed interface. The TKE budget is a key tool for understanding the turbulence processes and scales throughout the water column. Most open-channel flow studies over both smooth and rough beds locate the maximum TKE production and turbulent diffusion at the bed (Nezu & Nakagawa 1993; Song, Graf & Lemmin 1994; Balachandar & Bhuiyan 2007). This is mainly due to the poor resolution close to and within the roughness elements. However, Lopez & Garcia (2001) measured flow properties both above and within a vegetation canopy and showed that the peak of turbulence activity occurs in the vicinity of the canopy crest

in a very similar manner to rough atmospheric boundary layers (Raupach, Antonia & Rajagopalan 1991; Finnigan 2000). Hence, the spatially averaged TKE production reaches a maximum near the upper part of the roughness elements. Most studies on rough open-channel flow also indicate an upward vertical kinetic energy flux at all elevations above the bed, while few other studies (Lopez & Garcia 1999; Hurther & Lemmin 2000; Hurther, Lemmin & Terray 2007) measured mean TKE fluxes oriented towards the bed in the inner flow region defined as $z/h < 0.2$. These hydrodynamic aspects are the first strong motivation for our experimental study. Therefore the first objective of the present study is the experimental analysis of the TKE budget for rough open-channel flows over large gravel elements which, to our knowledge, has not yet been measured and analysed with sufficient spatial resolution in the near-bed region.

Buffin-Belanger & Roy (1998) proposed a detailed mixing layer explanation of the turbulence properties around submerged large-scale macro-roughness bed elements. Moreover, several researchers (Raupach *et al.* 1991; Finnigan 2000; Nepf & Ghisalberti 2008) have also introduced the analogy between the turbulence over the canopy and the mixing layer theory, with the mixing plane located at the crest of the canopy, which is consistent with maximum TKE production roughly at this level. The second objective of this paper is to investigate whether the mixing layer analogy applies to open-channel-flow configurations over a bed with macro-roughness bed elements. Furthermore, the turbulent structure in flows over macro-roughness bed elements is expected to have strong similarities with flow properties around individual obstacles. Nelson, McLean & Wolfe (1993) showed that increased shear stress and TKE production occurs in the wake of the fixed obstacle. Buffin-Belanger & Roy (1998) found that for natural river flows, turbulence activity increases just downstream of pebble clusters in natural flows with low relative submergence. Moreover, Hoover & Ackerman (2004) suggest defining three classes of vertical turbulence characteristics, depending on their location with regard to the macro-roughness elements (also called bed protuberances). The third objective of the paper is therefore the characterization of local flow patterns into distinct classes and their contribution to the double-averaged TKE budget.

2. Experimental set-up

The experiments are conducted at the LEGI (Grenoble, France), in a 35 cm wide, 9 m long rectangular flume with a slope S_0 of 0.2 %. At the upstream end, a reservoir collects the discharge provided by the pump, and a honeycomb stabilies the flow entering the flume. A thin vertical weir at the downstream end ensures a subcritical uniform flow in the measuring section located 4 m from the channel entrance. Flow uniformity was checked by measuring the water surface mean slope over a streamwise distance of 8 m along the centreline of the channel. The mean hydraulic parameters of this reference flow case, named 'Case 1', are given in table 1. The bed is composed of about two layers of angular gravel elements (stones) of $d_{50} = 2$ cm which were deposited randomly on the bottom of the channel without any specific arrangement (figure 1). The irregular arrangement of the sediment on the bottom results in localized macro-roughness elements (composed of a few stones) protruding well above the mean bottom elevation. The irregular arrangement of the sediments on the bottom reveals random variations of bed elevation at the scale of the gravel elements (see figure 7). The presence of two larger localized macro-roughness bed elements with a length scale of 10 cm, composed of several gravel elements, can also

	S_0 (%)	Q ($l\,s^{-1}$)	h (cm)	U ($m\,s^{-1}$)	Re	Fr	u_* ($m\,s^{-1}$)	Re_*	z_0 (mm)	k_s (cm)	k_s^+	z_c (cm)	λ (mm)	η (mm)
Case 1	0.2	40.4	18.7	0.62	115400	0.46	0.053	9911	0.37	1.1	583	2.8	4.71	0.11
Case 2	0.2	40.4	16.9	0.68	115400	0.53	0.051	8619	0.28	0.52	265	1.2	4.77	0.11

TABLE 1. Hydraulic parameters: S_0 channel slope, Q discharge, h water depth (measured as the distance between z_c and the water surface), U bulk velocity, $Re = Uh/\nu$ Reynolds number, $Fr = U/(gh)^{1/2}$ Froude number, u_* friction velocity, $Re_* = u_* h/\nu$ friction Reynolds number, z_0 roughness length, k_s Nikuradse equivalent roughness size, $k_s^+ = u_* k_s/\nu$ roughness Reynolds number, z_c sediment crest level, $\lambda = (15\,\nu\langle\overline{u'^2}\rangle/\langle\epsilon\rangle)^{1/2}$ spatially averaged Taylor scale computed at $z = z_c$, $\eta = (\nu^3/\langle\epsilon\rangle)^{1/4}$ spatially averaged Kolmogorov scale computed at $z = z_c$.

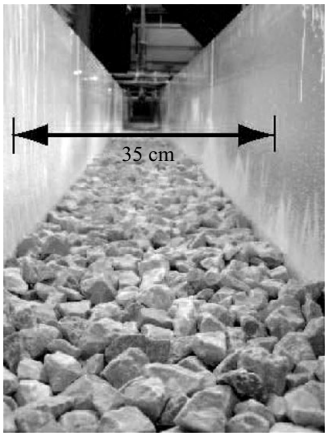

FIGURE 1. Upstream view of the flume with gravel sediment at the bottom.

be seen in figure 7. The gravel elements did not move during the tests, since the Shields parameter was far below its critical value for motion inception.

The studied area is located between $x = 4$ m and 4.9 m downstream from the channel entrance. This ensures a fully developed boundary layer and uniform flow over the entire measuring section (1 m long). This also ensures a sufficient distance from the downstream weir in order to have a flow independent of the downstream boundary condition. The bed topography is surveyed along the centreline of the channel. The bed elevation is measured every 1 cm with a digital point gauge with an accuracy of ± 0.5 mm. The reference plane $z = 0$ is defined as the average measured bed elevation, and z_c is the roughness crest level defined as the maximum bed elevation above the reference plane (see table 1 and figure 19).

As will be shown in the following section, the flow measurements are performed with a high-resolution three-axis Acoustic Doppler Velocity Profiler (ADVP) on the centreline of the channel. This measuring tool has been used extensively in the past 10 years for detailed turbulence studies in open-channel flows (Song *et al.* 1994; Hurther & Lemmin 2000, 2003; Blanckaert & de Vriend 2004, 2005; Hurther *et al.* 2007). Its use for the study of near-bed hydrodynamics is of particular interest here because the velocity at turbulent scales could be measured above and within the flow/bed interface, as will be shown in the following section. The ADVP is a high-resolution pulse-to-pulse coherent Doppler velocity system profiling simultaneously and quasi-instantaneously four radial velocity components in different directions along an

insonified water column about 20 cm below the emitter. The insonified water column can be approximated by a conical vertical beam with a diameter of about 2 cm (−6 dB limit) at the furthest sample volume located 6 mm from the local bed interface (one sample volume is lost due to bed reflection). It has been shown in Hurther & Lemmin (2001, 2008) that spatial averaging appears in the turbulent spectra above 20 Hz, allowing accurate estimations of velocity fluctuations linked to flow scales in the cm range. The emitter and the four receivers are placed in the water just below the free surface in order to form two pairs of bistatic systems. One pair is parallel to the streamwise direction for the measurement of u and w components, and the second pair is perpendicular to the streamwise direction for the measurement of the v and a redundant w velocity components. The introduction of the four transducers below the free surface induced flow disturbances over the first 4 cm. The first gate in the profiles is located at a distance of 8 cm and 7 cm below the emitter for flow Cases 1 and 2, respectively. The emitter generates pulse trains at 1.25 MHz with a duration of 4 μs at a pulse repetition frequency (PRF) of 1.5 kHz. Using the speed of sound in water, this results in sample volumes of vertical length equal to 3 mm. The local quasi-instantaneous radial velocity for each sample volume is calculated from the time derivative of the Doppler phase shift between the backscattered and the transmitted pulse, using a first-order backward step, finite difference scheme. In order to reduce the Doppler phase noise contribution linked to the random stationary backscattering process, the imaginary part of the auto-correlation function of the complex Doppler signal is calculated (Serafin & Lhermitte 1984; Hurther & Lemmin 2001, 2008). The optimum algorithm configuration in our flow conditions uses 32 consecutive echoes for one quasi-instantaneous velocity estimation at each sample volume. As a result the temporal resolution becomes $32/\mathrm{PRF} = 32/1500 = 21.33\,\mathrm{ms} \simeq 146.9\,\mathrm{Hz}$. The water in our open channel is naturally saturated with micro air bubbles thanks to the re-aeration of the falling water at the downstream end of the channel. This offers ideal acoustic backscattering conditions avoiding any adjunction of seeding particles. As previously shown by Shen & Lemmin (1997) these micro air bubbles have negligible inertial lag over the bandwidth resolved by the ADVP. The u, v and w velocity components are reconstructed from the geometrical combination of the radial velocity components, using triangulation to calculate of the local Doppler angles and the positions of the gates (or sample volumes) relative to the emitter. For the flow conditions studied here the spatio-temporal resolution is sufficient to estimate the Taylor microscales, whereas the Kolmogorov scale cannot be resolved (see table 1). Moreover, the time-averaged quantities presented in the following sections were all calculated from data samples of 300 s duration. The uncertainties in velocity variances and Reynolds stress for this record length were estimated to be less than 20 %. The measurement uncertainties for the TKE production and the TKE flux terms are very similar due to the negligible errors in the mean velocity estimation and the intrinsic covariances and tri-variances contained in these terms. Nevertheless, the diffusive TKE transport term suffers from the vertical gradient estimation but should also not exceed 30 % because the tri-variance calculation is weakly affected by noise, specifically when the Doppler noise is fairly white over the resolved bandwidth (Hurther & Lemmin 2001).

To summarize, in the present experiments the collected profiles extend over the lower half of the water column, with u, v, w, being the streamwise, the transverse and the vertical velocity components, respectively, along the x-, y- and z-axis. The profiles presented in the paper are obtained from a data set of time length equal to 300 s sampled at a frequency of 46.9 Hz. Vertical velocity profiles were measured at

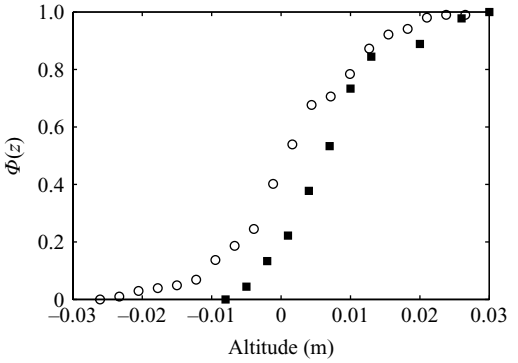

FIGURE 2. Roughness geometry function from the point gauge (○) and ADVP (■) topography measurements for Case 1.

45 different locations along the channel centreline inside the measurement section. Each vertical is separated by a fixed streamwise distance of 2 cm so that neighbouring measurement volumes do not overlap.

A peak detection method in the backscattered acoustic intensity was applied to locate the local gravel-bed interface with a resolution of a few millimetres in the vertical direction. The measure of the bottom elevation at the 45 locations allows the computation of the roughness geometry function (Nikora *et al.* 2001). The function $\Phi(z)$ is the fraction of fluid in a plane parallel to the flow direction at altitude z (Nikora *et al.* 2001). Figure 2 compares the roughness geometry functions $\Phi(z)$ obtained with the point gauge and the ADVP. It appears that the ADVP tends to overestimate the local-bed elevation due to the limited penetration depth of the acoustic beam in flow cavities between gravel elements that are smaller than the beam width.

3. Averaging methodology

Due to the large size of the gravel elements with regard to the small-scale flow eddies and their irregular arrangement on the bottom, the time-averaged flow characteristics close to the bed are three-dimensional. In order to bridge the gap between local descriptions of the flow and the large-scale information required for engineering applications, spatial averaging is useful. Spatial averaging of the flow quantities is applied over surfaces with a longitudinal and transverse size greater than the horizontal length scale of the roughness elements but small enough so that the differences in elevation, due to the overall bed slope, within the averaging surface can be neglected. For our purpose, the main interest of spatial averaging lies in the estimation of the averaged spatial deviations of the turbulence characteristics from their time and spatial averages. These spatial deviations are paramount for the analysis of energy-related quantities within the bed roughness.

The starting point is the Reynolds decomposition of the instantaneous velocity component into $u_i = \bar{U}_i + u_i'$, with $\bar{U}_i$ the time-averaged velocity for the velocity component in direction i. The time fluctuating contribution is u_i'. Plane-averaged quantities (Wilson & Shaw 1977) are noted using angle brackets, $\langle\,\rangle$, in the equations given below. As highlighted by Nikora *et al.* (2007), two different spatial averages are considered. The first is the so-called intrinsic spatial average and is expressed as

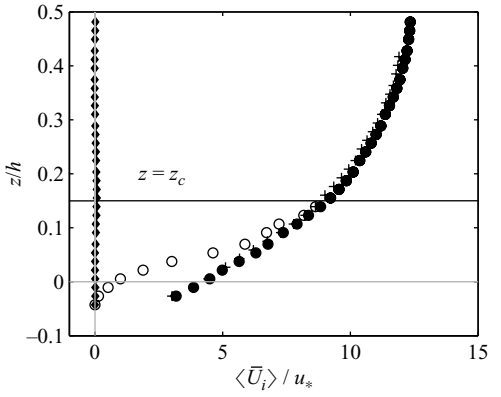

FIGURE 3. Intrinsic (●) and superficial (○) double-averaged streamwise velocity of the studied zone (x between 4.0 m and 4.9 m) with intrinsic averaged velocity (+) for the downstream zone (x between 5.5 and 5.7 m) and superficial double-averaged vertical velocity (◆) (Case 1).

follows when applied to $\overline{U_i}$:

$$\langle \overline{U_i}(\boldsymbol{x}, t) \rangle = \frac{1}{A_f} \iint_{A_f} \overline{U_i}(\boldsymbol{x} + \boldsymbol{r}, t)\, \mathrm{d}S. \tag{3.1}$$

The second average is the so-called superficial spatial average (Nikora *et al.* 2007):

$$\langle \overline{U_i}(\boldsymbol{x}, t) \rangle_s = \frac{1}{A_0} \iint_{A_f} \overline{U_i}(\boldsymbol{x} + \boldsymbol{r}, t)\, \mathrm{d}S, \tag{3.2}$$

where A_f is the area occupied by the fluid at a given altitude z within A_0, the total averaging plane area at this given altitude; $\boldsymbol{r}$ is the vector describing A_f around location point $\boldsymbol{x}$ and $\mathrm{d}S$ is an infinitesimal area element. Above z_c, A_f is equal to A_0 and $\langle \bar{U}_i \rangle_s = \langle \bar{U}_i \rangle$. Below z_c, the roughness geometry function can be written as $\langle \bar{U}_i \rangle_s = \Phi(z) \langle \bar{U}_i \rangle$. Based on the intrinsic average, the following decomposition of the local mean velocity component is introduced:

$$\overline{U_i} = \langle \overline{U_i} \rangle + \tilde{u}_i, \tag{3.3}$$

where $\tilde{u}_i$ is the deviation of the local time-averaged velocity from the double-averaged velocity $\langle \overline{U}_i(z) \rangle$. By definition, $\langle \tilde{u}_i \rangle = 0$. By extension any flow quantity θ can be decomposed as,

$$\overline{\theta} = \langle \overline{\theta} \rangle + \tilde{\theta}. \tag{3.4}$$

For the setting considered, the roughness geometry function is shown in figure 2. The superficial DA at a given altitude was performed by summing the fluid velocities measured at this elevation over the 45 profiles and dividing by 45. Flow uniformity at a larger scale was checked by measuring 20 additional turbulent profiles 50 cm downstream of the measuring section between $x = 5.5$ m and 5.7 m. Figure 3 shows very good agreement between the intrinsic average velocity profiles, confirming the large-scale flow uniformity. This also shows that 20 cm should be enough for double-averaged streamwise velocity estimations.

Figure 3 shows how the averaging method affects the double-averaged streamwise velocity component. The superficial double-averaged velocity drops to zero more rapidly than the intrinsic double-averaged velocity within the roughness layer due to the rapid decrease in fluid fraction area with decreasing z. As a result, the inflectional

shape seen in the superficial double-averaged profile is an effect of the roughness geometry function rather than the signature of the possible mixing-layer-type nature of the near-bed flow. The quasi-linear trend of the intrinsic averaged velocity below $z_c = 0.15\,h$ is in good agreement with the prediction for large depth-to-roughness ratio ($h/d_{50} \sim 8$) of type 1 flow defined by Nikora *et al.* (2001) and Nikora *et al.* (2004). By itself this linear trend shows that, within the roughness layer, the fluid velocity is retarded with respect to the log type profile of a smooth hydraulic flow. However, this is in contrast with the vegetation canopy case (Lopez & Garcia 2001) for which $\Phi(z)$ is quasi-constant and close to unity, resulting in very close intrinsic and superficial averages. Finally, for $z > z_c$ both double-averaged velocities coincide, since $\Phi(z) = 1$.

The friction velocity u_* is determined from a Clauser-type analysis on the double-averaged velocity profile. This approach is chosen because it does not require *a priori* definition of the zero-displacement plane. In contrast, the method based on Reynolds shear stress requires the choice of an elevation at which this shear stress should be extrapolated. We thus proceed by fitting above z_c the double-averaged velocity profile data with the following logarithmic law (Millikan 1938):

$$\frac{\langle \bar{U}(z) \rangle}{u_*} = \frac{1}{\kappa}\,\ln\left(\frac{z+\Delta z}{k_s}\right) + B \text{ or equivalently } \frac{\langle \bar{U}(z) \rangle}{u_*} = \frac{1}{\kappa}\,\ln\left(\frac{z+\Delta z}{z_0}\right) \tag{3.5}$$

with $\kappa = 0.41$ the von Karman constant; u_*, Δz, k_s and z_0 are all determined during the fitting process. The equivalent Nikuradse roughness size k_s obtained, which is a virtual measurement, is of the same order of magnitude as the standard deviation σ_z of the bottom elevations which is calculated at a value of $\sigma_z = 0.74$ cm. The roughness Reynolds number $k_s^+ = u_* k_s/\nu$ (see table 1) confirms that our regime is completely rough ($k_s^+ \gg 70$). Note that the universality of the log law was once more confirmed for organized rough boundary layers by Castro (2007). The displacement height Δz was found to be very small, $\Delta z \simeq -0.15\,k_s$, or roughly 1 mm. The Nikuradse zero-plane displacement is therefore located at the mean bed elevation.

4. Velocity moments and class analysis

4.1. *Spatially averaged basic turbulence characteristics*

The double-averaged momentum equation will be presented in this section. It is of common knowledge that three-dimensional effects are present in channel flows especially for small width-to-depth ratios, in the form of at least two counter-rotating cells in each cross-section. Indeed, two symmetrical cells with respect to the flume centre-plane were observed in our cases. However, the influence of such cells could not be measured due to experimental limitations.

The double-averaged momentum equation for uniform two-dimensional open-channel flow (4.1) has been written by various researchers such as Nikora *et al.* (2001, 2004) and Lopez & Garcia (2001). It reads:

$$\frac{\partial}{\partial z}\left(\overbrace{\mu\,\frac{\partial \langle \bar{U} \rangle_s}{\partial z}\underbrace{-\rho\langle \overline{u'w'} \rangle_s - \rho\langle \tilde{u}\tilde{w} \rangle_s}_{\tau_t}}^{\tau}\right) - \rho g\, S_0\, \Phi(z) + (f_p(z) + f_v(z)), \tag{4.1}$$

where f_p and f_v are the drag forces induced respectively by the pressure and the viscous forces integrated on the contours of the roughness elements. Consequently, $(f_p + f_v)$ disappears for values of z above z_c. Moreover, the second term on the

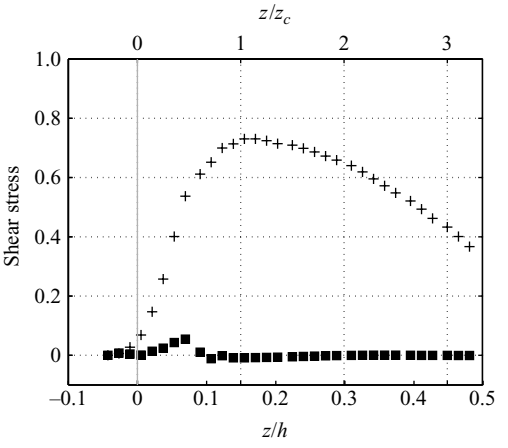

FIGURE 4. Non-dimensional superficial double-averaged τ_t shear stress terms. (+): $-\langle\overline{u'w'}\rangle_s/u_*^2$; (■): $-\langle\tilde{u}\tilde{w}\rangle_s/u_*^2$.

left-hand side written with tildes is an additional bed-form-induced shear stress or dispersive stresses. The sum of the three flow resistance terms is defined as the total shear stress τ next.

Integration of (4.1) gives the total shear stress for $z > z_c$,

$$\tau(z) = \rho g\, S_0(h - z), \tag{4.2}$$

which shows that, above z_c, the total shear stress is linear as expected and as found experimentally by Lopez & Garcia (2001) for vegetation canopies in open-channel flows. For $z < z_c$

$$\tau(z) = \rho g\, S_0\,(h - z_c) + \rho g\, S_0 \int_z^{z_c} \Phi(z)\,\mathrm{d}z - \int_z^{z_c} \left(f_p + f_v\right)\,\mathrm{d}z. \tag{4.3}$$

The double-averaged technique applied to the Reynolds equation therefore generates a bed-form-induced shear stress (Nikora *et al.* 2001).

The different terms of (4.1) are evaluated from our measurements and are presented hereafter. Figure 4 shows that in Case 1 flow, this measured additional shear stress $\langle\tilde{u}\tilde{w}\rangle_s$ is negligible above z_c and that it is much smaller than the classical turbulent shear stress component $\langle\overline{u'w'}\rangle_s$ below z_c. The maximum value of the bed-form induced shear stress term is about $0.06\,u_*^2$ which is consistent with the measurements by Nikora *et al.* (2001) for a similar Reynolds number of $Re \equiv 10^5$ but lower than those of Manes, Pokrajac & McEwan (2007) for a lower Reynolds number of $Re \equiv 10^4$. Coceal *et al.* (2006) with direct numerical simulation (DNS) calculations for a flow over an staggered cubical urban canopy found a maximum value of the dispersive stresses of about $0.15\,u_*^2$ which is more than twice our value. The viscous term in $\tau(z)$ is negligible with regard to the main Reynolds shear stress term (not shown here).

Many reports of measurements of the turbulent intensity profiles for various rough flow regimes of different roughness Reynolds number k_s^+ can be found in the literature (Nezu & Nakagawa 1993; Hurther & Lemmin 2001; Nikora *et al.* 2001; Bigillon, Nino & Garcia 2006). The data in figure 5 are consistent with those reported earlier in the literature cited. The maximum values of turbulent intensities are reached slightly below z_c and drop rapidly to zero below z_c due to the superficial averaging. However, note that the maximum value for the vertical intensity is equal to 0.56. This is in

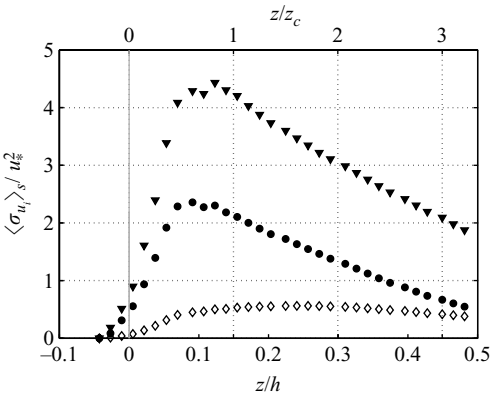

FIGURE 5. Superficial double-averaged turbulent intensities. (▼): $\langle\sigma_u\rangle_s/u_*^2$; (●): $\langle\sigma_v\rangle_s/u_*^2$, (◇): $\langle\sigma_w\rangle_s/u_*^2$.

agreement with measurements by Nikora *et al.* (2001) and Franca (2005*a*) for flows over large roughness elements, whereas measurements for smaller roughness elements by Nezu & Nakagawa (1993) for $0 < k_s^+ < 136$ and Bigillon *et al.* (2006) for $k_s^+ = 10$ reach a value close to 1.

4.2. *Local flow characterization and classification*

The previous analysis discussed double-averaged properties of the gravel-bed channel flow across and above the flow/bed interface. However this global methodology tends to integrate the detailed dynamics. In this part local characterization of the flow will be associated with the double-averaged one. Hoover & Ackerman (2004) proposed a classification of the flow characteristics in different classes, depending on the properties of the local time-averaged velocity profiles. They suggested defining three classes of velocity profiles around an individual macro-roughness bed elements with very low relative submergence: the 'logarithmically distributed', the 'S-shaped' and the 'wedge-shaped' profiles. Similar tendencies were also reported for higher relative submergences (Coceal *et al.* 2006, 2007*c*; Franca 2005*b*; Nelson *et al.* 1993).

The purpose of this section is to verify whether this local flow characterization can be applied to the studied flow conditions and to potentially combine it with the results of the DA method. For the first class (called 'log' profiles hereafter), the mean streamwise velocity fits a logarithmic curve over almost the entire measured profile (see figure 6). The second class called S-shaped refers to profiles that can be encountered in the wake of macro-roughness bed elements due to flow separation on the lee side. These particularly important velocity profiles exhibit an inflexional behaviour specific to retarded flows as in confined detached flows that are also very similar to mixing layers. Finally, the last class called accelerated profiles (similar to the wedge-shaped profiles defined by Hoover & Ackerman 2004) consists of profiles located in the vicinity of the top of the macro-roughness elements. The associated velocities are slightly higher than the log class ones above z_c and rapidly drop to zero at or slightly below the top of the highest roughness element ($z = z_c$). Consequently, these profiles never extend down to the reference plane $z = 0$. Figure 6 shows the plot of three local mean velocity profiles, and it can be seen that, above z_c, where they are not influenced by the bed heterogeneity, all classes behave quite similarly. Below z_c, they differ significantly. Of the 45 profiles the following class distribution was obtained: 24 are log profiles; 12 are S-shaped profiles; and 9 are accelerated profiles.

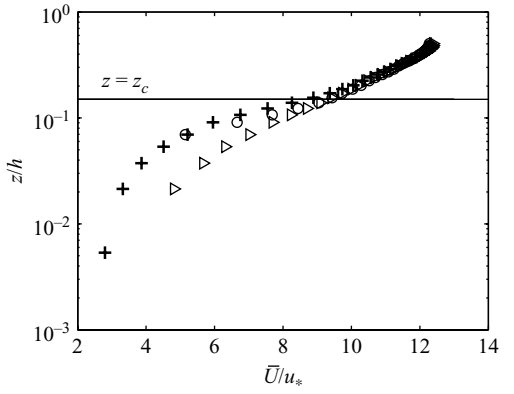

FIGURE 6. Examples of local profiles of time-averaged streamwise velocity chosen in each of the three classes for Case 1. (▷): log; (+): S-shaped; (○): accelerated.

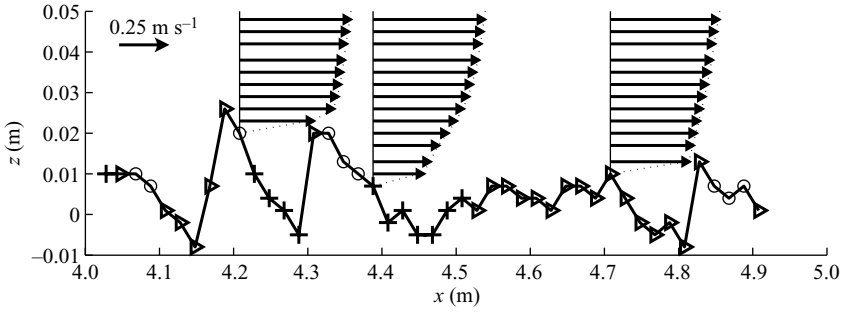

FIGURE 7. Local mean streamwise velocity from ADVP measurements and bed topography. Profiles are associated with a symbol, drawn at the bottom, representing one of the three classes to which they pertain: (▷) log; (+) S-shaped; (○) accelerated.

Figure 7 shows the plot of three typical profiles of each class and the streamwise locations of the 45 equally spaced profiles above the gravel–fluid interface topography along with the labels indicating their class. The spatial distribution of the labels is obviously closely related to the location with regard to the macro-roughness bed elements. In the zones with low local bed gradients ($x \sim 4.5$–4.8 m), all the profiles belong to the log class. In contrast, close to the top ($x \sim 4.3$–4.35 m) and downstream from the highest gravel elements ($x \sim 4.2$–4.3 or 4.35–4.5 m), the profiles belong to the accelerated and S-shaped classes, respectively. This confirms the trend observed by Hoover & Ackerman (2004) in the vicinity of a single macro-roughness bed element.

Superficial DA is performed per class, using the same method as for the total superficial DA. The turbulent shear stress τ_t for each class is computed and plotted in figure 8. It is clearly apparent that the three class-averaged shear profiles and the overall superficial average for the 45 profiles have the same behaviour above $z/h = 0.3$. In contrast, at and below z_c, the S-shaped superficially averaged shear stress has an overshoot and reaches its maximum value at $z/z_c \sim 0.5$ (similar to Nelson *et al.* 1993) becoming much stronger than those of the log class and accelerated class. It is also apparent that the superficial log class shear profile is quite close to the total superficial double-averaged shear stress profile.

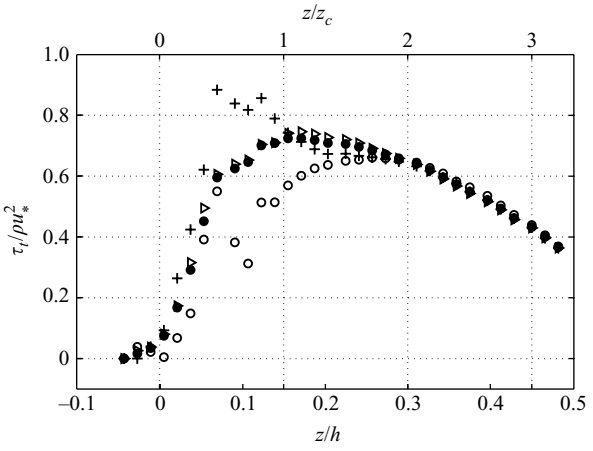

FIGURE 8. Superficial double-averaged shear stress τ_t per class. (▷): log; (+): S-shaped; (○): accelerated; (●): all 45 profiles.

5. The TKE budget

5.1. *The double-averaged TKE budget*

The DA of the TKE budget equation can be written as (see for instance Mignot, Barthélemy & Hurther 2008)

$$-\Phi(z)\,\langle\overline{u_i'u_j'}\rangle\,\frac{\partial\langle\overline{U_i}\rangle}{\partial x_j}-\Phi(z)\,\langle\overline{u_i'u_j'}\rangle\,\left\langle\frac{\partial\tilde{u}_i}{\partial x_j}\right\rangle-\Phi(z)\left\langle\widetilde{u_i'u_j'}\,\frac{\partial\tilde{u}_i}{\partial x_j}\right\rangle=\Phi(z)\,\langle\epsilon\rangle$$
$$+\frac{\partial\Phi(z)\langle k\rangle\langle\overline{U_j}\rangle}{\partial x_j}+\frac{\partial\Phi(z)\langle\tilde{k}\tilde{u}_j\rangle}{\partial x_j}+\frac{\partial}{\partial x_j}\left(\Phi(z)\langle\overline{k'u_j'}\rangle+\frac{\Phi(z)}{\rho}\langle\overline{p'u_j'}\rangle\right)-\Phi(z)\nu\,\langle\nabla^2 k\rangle \tag{5.1}$$

with i and $j=1, 2, 3$ referring to x-, y- and z-axis respectively.

This double-averaged budget was derived by Raupach *et al.* (1991) for a permanent fully developed two-dimensional flow over a vegetation canopy. However, in our case, the bottom conditions give a $\Phi(z)$ function of z (see figure 2). Consequently, this double-averaged TKE budget (5.1) for a simplified uniform flow over a gravel-bed becomes

$$\underbrace{-\langle\overline{u'w'}\rangle_s\,\frac{\partial\langle\bar{U}\rangle}{\partial z}}_{P}-\left[\underbrace{\langle\overline{u_i'u_j'}\rangle_s\left\langle\frac{\partial\tilde{u}_i}{\partial x_j}\right\rangle}_{P_m}+\underbrace{\left\langle\widetilde{u_i'u_j'}\,\frac{\partial\tilde{u}_i}{\partial x_j}\right\rangle_s}_{P_w}\right]$$
$$=\langle\epsilon\rangle_s+\underbrace{\frac{\partial}{\partial z}\left[\underbrace{\langle\overline{k'w'}\rangle_s}_{F_k}+\underbrace{\langle\tilde{k}\tilde{w}\rangle_s}_{F_w}\right]}_{T_T}+\frac{1}{\rho}\frac{\partial\langle\overline{p'w'}\rangle_s}{\partial z}-\nu\,\frac{\partial^2\langle k\rangle_s}{\partial z^2}. \tag{5.2}$$

The TKE production term P is due to the work of the double-averaged velocity against the double-averaged shear; P_w is the TKE production rate resulting from the work of the wake-induced velocity fluctuations against the bed induced shear, while P_m is the work of the bed-induced velocity fluctuations against the double-averaged

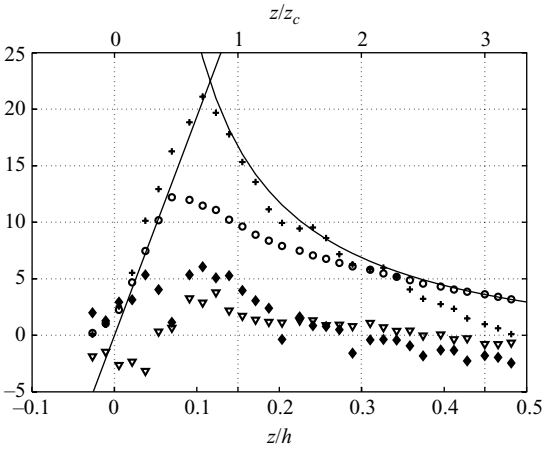

FIGURE 9. Double-averaged terms of the TKE budget for Case 1. Full lines refer to (5.3) for $z/z_c > 0.75$ and (5.4) for $z/z_c < 0.75$. (+): $P\,h/u_*^3$; (○): $\langle\epsilon\rangle_s\,h/u_*^3$; (▽): $T_T\,h/u_*^3$; (◆): $R\,h/u_*^3$ ($R = P - \langle\epsilon\rangle_s - T_t$).

shear stress. The terms on the right-hand side are (from left to right) the dissipation $\langle\epsilon\rangle_s$, the usual vertical TKE transport term $\partial F_k/\partial z$ induced by turbulent diffusion, the bed-form-induced $\partial F_w/\partial z$ turbulent diffusion, the pressure diffusion and finally the viscous dissipation term with $k' = (u'^2 + v'^2 + w'^2)/2$ and $k = \overline{k'}$. It was checked that the viscous dissipation term can be discarded with regard to the other terms throughout the water column. It should be noted that the TKE production term P_m does not appear in the Raupach *et al.* (1991) budget. This originates from the roughness geometry function in vegetation or urban canopies that is independent of z (Mignot *et al.* 2008).

The present section is devoted to the evaluation of these terms (when available) in order to compare the TKE budget in a gravel-bed open-channel flow to the ones in flows over vegetated canopies.

Of the 19 TKE production terms (9 for each bed-form induced term P_m and P_w plus the traditional 1 for P), only the 7 involving vertical derivatives ($j = 3$) can be directly estimated from our experimental data, as none of the streamwise and transverse derivatives can be estimated. However, it appears that the six estimated bed-form-induced terms can be neglected (as they remain lower than 5 % of the main TKE production term for the whole profile) with respect to the standard TKE production term P. This indicates that the terms P_m and P_w should be negligible in comparison to the term P for our bed conditions. This contrasts with the results obtained by Raupach *et al.* (1991) for wind above vegetation canopies. In their case P_w is far from being negligible below z_c. Lopez & Garcia (2001) did not measure the P_w term for water flows over plant canopies but gave numerical results obtained with a $k - \epsilon$ model. They found that P_w can be twice as strong as P within the roughness layer.

In figure 9, P reaches a maximum value slightly below z_c, at $z/z_c = 0.75$ similar to Raupach *et al.* (1991) and Lopez & Garcia (2001). Below this level, P decreases towards a value close to zero for $z/h = 0$ (figure 9). The maximum TKE production occurs at elevations that are in agreement with DNS computations by Le, Moin & Kim (1997) for the case of reattached mixing layers created in flows over backward-facing

steps. This latter type of flow has strong similarities with regions in our flows in which the flow detaches at the top of the macro-roughness bed element.

In fact the functional form of P and its maximum value can be deduced from turbulence 'first principles'. Assuming a shear stress linear above z_c in the log layer, the following equation can be written:

$$P = -\langle\overline{u'w'}\rangle_s \frac{\partial\langle\bar{U}\rangle}{\partial z} = -\langle\overline{u'w'}\rangle \frac{\partial\langle\bar{U}\rangle}{\partial z} = \frac{u_*^3}{\kappa z}\left(1 - \frac{z - z_c}{h - z_c}\right), \tag{5.3}$$

which is an adaptation to gravel bed open-channel flows of Nakagawa, Nezu & Ueda (1975) (cited in Nezu & Nakagawa 1993, p. 23). The trend of P obtained in figure 9 for $0.75 < z/z_c < 2$ is in good agreement with (5.3). The outskirts values of relation (5.3) could probably be improved to match the data more closely if the law of the wake were taken into account for the outer region.

In the central part of the roughness interface ($0 < z/z_c < 0.75$) our superficial double-averaged shear stress profile is close to linear (figure 4) which is in agreement with model 3 discussed by Nikora *et al.* (2004). Moreover, considering the linearity of the intrinsic spatial average velocity profile shown in figure 3, the TKE production should also be linear in this region. Finally, since the TKE production P is negligible at the reference plane $z = 0$ and that it must match its maximum value at the top of the layer, slightly below z_c, the following expression of P below z_c can be proposed:

$$\frac{Ph}{u_*^3} \simeq \frac{1.78}{\kappa}\left(\frac{h}{z_c}\right)\left(\frac{z}{z_c}\right). \tag{5.4}$$

The data in figure 9 strongly support this linear relationship (5.4). Note that relations (5.3) and (5.4) intersect at $z/z_c \simeq 0.75$, estimating a maximum TKE production value in agreement with the measurements.

Concerning the turbulent diffusion terms, Raupach *et al.* (1991) observed that the bed-form-induced term $\partial F_w/\partial z$ can be neglected when compared with the standard $\partial F_k/\partial z$ term. Such a result is also found in our experimental data. The standard wall normal TKE flux term F_k is calculated directly from the data without any approximation, since the ADVP provides all three fluctuating velocity components. The three terms constituting F_k are plotted in figure 10. Our data show that $\langle\overline{w'u'^2}\rangle_s$ is the main contribution to F_k. This term has negative values near the wall with a minimum value of roughly -0.2, in close agreement with measurements taken by Antonia & Krogstad (2001) for different type of roughness. The $\langle\overline{w'^3}\rangle_s/2u_*^3$ contribution is also negative in the near-wall region but with a higher value of -0.02 compared to the value obtained by Antonia & Krogstad (2001) for their case of two-dimensional rod-type roughness.

For measurements limited to two components (in streamwise and vertical directions), as is often the case in the literature, the term $\langle\overline{w'v'^2}\rangle_s$ is not measured, and the approximation $\langle\overline{w'v'^2}\rangle_s \approx \langle\overline{w'^3}\rangle_s$ is sometimes considered (Nakagawa & Nezu 1977). This approximation is reasonable for our conditions except over the range $1 < z/z_c < 2$ (see figure 10). Indeed close to z_c, $\langle\overline{w'v'^2}\rangle_s$ is the dominant contribution to F_k, since the two other contributions are close to zero. Hence, this frequently used approximation can lead to underestimations of F_k in the vicinity of z_c (see figure 10).

In addition our data yield linear relationships between third-order moments as shown in figure 11 in which the following notations are used for the non-dimensional

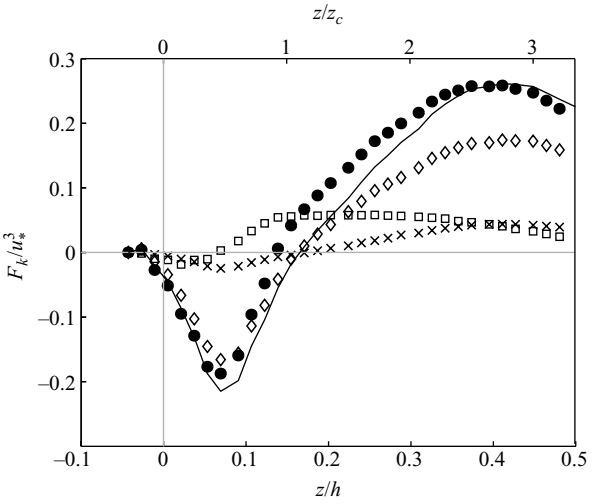

FIGURE 10. Third-order moment contributions to TKE wall normal fluxes. (●): F_k/u_*^3; (◇): $\langle\overline{u'^2w'}\rangle_s/2u_*^3$; (×): $\langle\overline{w'^3}\rangle_s/2u_*^3$; (□): $\langle\overline{v'^2w'}\rangle_s/2u_*^3$. Full line is the double-averaged flux computed with the assumption $\langle\overline{w'v'^2}\rangle_s = \langle\overline{w'^3}\rangle_s$.

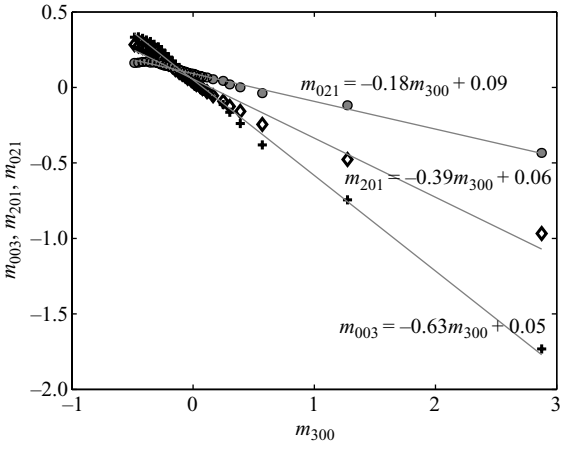

FIGURE 11. Dimensionless third-order velocity moments. Values of the linear fits between the third-order moments and m_{300} are given.

third-order moments:

$$m_{ijk} = \frac{\langle\overline{u'^i\, v'^j\, w'^k}\rangle}{u^i_{rms}\, v^j_{rms}\, w^k_{rms}}. \tag{5.5}$$

A similar linear relation was already revealed by Raupach, Antonia & Rajagopalan (1981) for wind tunnel experiments and Hurther & Lemmin (2000) for transitionally rough flows, and it appears that they also apply to fully rough flow conditions. The ratios between m_{003}, m_{201} and the streamwise skewness m_{300}, are very close to those found by Raupach *et al.* (1981).

The data for F_k in figure 10 are positive above z_c with a maximum value of approximately $0.25\,u_*^3$ away from z_c. This value is close to the values obtained by Lopez & Garcia (1999), Hurther & Lemmin (2000) and Bigillon *et al.* (2006). At

z_c, the flux is close to zero with a maximum slope resulting in strong diffusional TKE transport. Below z_c, the flux becomes negative with a minimum value of about $-0.2\,u_*^3$ at roughly $z_c/2$ and then increases towards zero close to the reference plane. Similar tendencies are seen in fully rough beds studies such as those by Raupach *et al.* (1991), Hurther & Lemmin (2000) and Lopez & Garcia (2001). This is in strong contrast with measurements of flows over beds that are smooth or with very little roughness in which the flux term is never oriented towards the bed (Lopez & Garcia 1999; Hurther & Lemmin 2000; Bigillon *et al.* 2006). Finally, the double-averaged dissipation $\langle\epsilon\rangle_s$ is a key element in the TKE budget. Figure 9 shows the measurement of the double-averaged dissipation across and above the flow/bed interface computed by the standard macroscale approach,

$$\epsilon = C_1 \frac{(\overline{u'^2})^{3/2}}{L_x}, \tag{5.6}$$

where C_1 is a constant set to unity for our open-channel flow conditions (Nezu & Nakagawa 1993, (2.39), p. 22) and L_x is the turbulent streamwise macroscale; $L_x(z) = L_t(z)\overline{U}(z)$ with $L_t(z)$ the Lagrangian integral time scale (integral of the normalized temporal local autocorrelation function of the streamwise fluctuating velocity component (Nezu & Nakagawa 1993, p. 21 (2.36)) at each elevation). In order to increase the accuracy of the streamwise velocity variance estimation in relation (5.6), a Doppler noise suppression technique is applied, as originally proposed by Garbini, Forster & Jorgensen (1982). It consists of approximating the local velocity variance at gate j by the mean cross-product of the velocity fluctuation at two consecutive gates:

$$(\overline{u'^2})_j = \overline{u'_j\, u'_{j-1}}. \tag{5.7}$$

Because the distance between two consecutive gates is sufficiently small to resolve the turbulent micro-scales, the statistically independent Doppler noise between two consecutive gates is reduced significantly (Garbini *et al.* 1982; Hurther & Lemmin 2001, 2008). As a result, the measurement uncertainty of the TKE dissipation rate using the previous method should be less than 20 % as for the TKE production terms when the error on constant C_1 of (5.6) can be neglected.

The main features are that, above $2z_c$, $\langle\epsilon\rangle_s$ and P have similar magnitudes, giving some support to the presence of an equilibrium layer (Lopez & Garcia 1999, 2001; Hurther *et al.* 2007). This agrees with the data of Lopez & Garcia (2001) for water flows over plant canopies and also with those of Raupach *et al.* (1991). Close to z_c, TKE production exceeds dissipation by 80 %. DNS computations for reattached mixing layers at five times the step height downstream of the step give 25 % (Le *et al.* 1997), a much smaller value. The maximum dissipation occurs at a level $z_c/2$, lower than that of the maximum TKE production P. This shift is also noticeable in DNS computations of reattached mixing layers. Below $z_c/2$, the TKE production and dissipation terms are again very similar. Consequently,

(*a*) the large excess of turbulent kinetic energy generated in the vicinity of z_c must be transported away both upward and downward by the turbulent diffusion T_T; nevertheless, the contribution of pressure diffusion cannot be excluded; and

(*b*) given that in uniform flows, $\int_{depth} P\,\mathrm{d}z = \int_{depth}\langle\epsilon\rangle_s\,\mathrm{d}z$, and as P exceeds $\langle\epsilon\rangle_s$ at $z \equiv z_c$, $\langle\epsilon\rangle_s$ must exceed P somewhere in the higher fluid layers. This behaviour is noticeable in figure 9.

In order to give a complete view of the budget, figure 9 shows the residue $R = P - \langle\epsilon\rangle_s - T_T$ often associated with pressure transport which is never measured

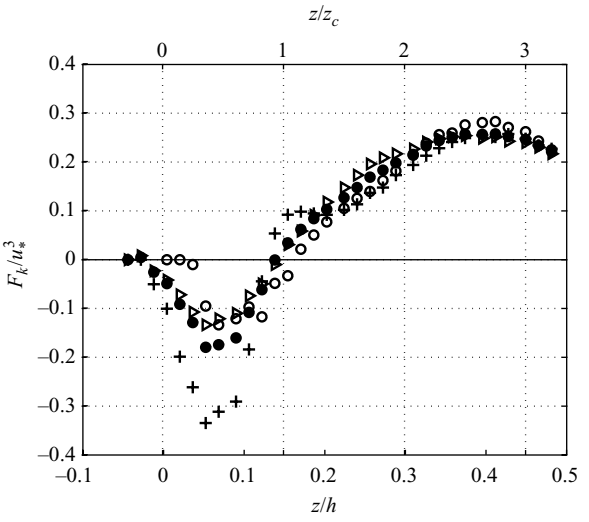

FIGURE 12. Superficial double-averaged TKE flux F_k per class. (▷): log; (+): S-shaped; (○): accelerated; (●): all 45 profiles.

directly. Within the roughness interface this residue is of the same order of magnitude as T_T. However in the lower part of the roughness layer where all measured quantities are small, the residue R should contain relatively significant errors. The question of the sign of pressure transport in the upper part of canopies is still open (Finnigan 2000).

5.2. *Class contribution to the TKE budget*

As for the mean streamwise velocity and shear stress profiles, the presence of macro-roughness elements strongly modifies the TKE budget locally, especially in the roughness region. Superficial DA of the main TKE terms per class is analysed here with the same approach as in § 4.2.

It appears that, below z_c, the negative TKE flux ($F_k < 0$) directed towards the bed significantly increases in the wakes (related to the S-shaped class) in comparison to the total double-averaged TKE flux (figure 12). Moreover, it appears that the average log class negative TKE flux below z_c is small and less than the total double-averaged flux (25 % deviation), which clearly indicates that the presence of the macro-roughness bed elements (giving rise to the S-shaped flux terms) increases the energy flux directed towards the bed. Furthermore, figure 13 shows that the maximum TKE production occurs at the upper limit of the wakes, slightly below z_c for the three classes. The superficial S-shaped class double-averaged TKE production and dissipation values (figure 14) are almost twice as high as the total double-averaged TKE production, showing the importance of the wake contribution to the double-averaged TKE production and dissipation terms. These combined results of the TKE flux and the TKE production show that the S-shaped class imposes a strong signature on the double-averaged flow properties. As pointed out earlier, this is also the case for the DA streamwise velocity for which the S-shaped retarded flows averaged with the log class gives a quasi-linear velocity profile in the roughness. This reflects the analogy between highly rough flows with macro-roughness bed elements and mixing layer flows (Raupach, Finnigan & Brunet 1996). This is examined in detail

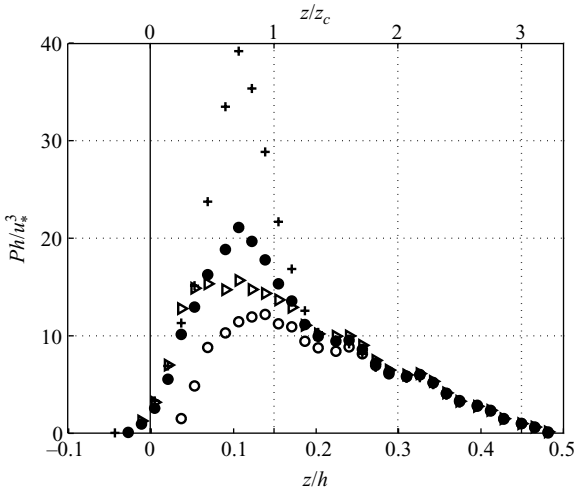

FIGURE 13. Superficial double-averaged TKE production P per class. (▷): log; (+): S-shaped; (○): accelerated; (●): all 45 profiles.

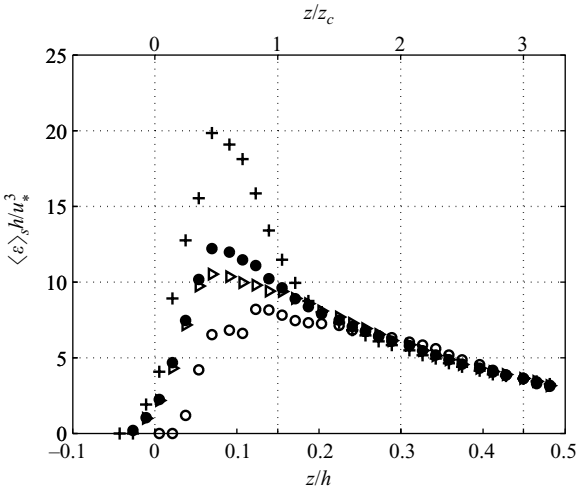

FIGURE 14. Superficial double-averaged dissipation $\langle\epsilon\rangle_s$ per class. (▷): log; (+): S-shaped; (○); accelerated; (●): all 45 profiles.

in the following section by analysing the spatial variation in energy-related turbulent quantities.

5.3. *Spatial variation in TKE quantities in wakes*

A typical spatial variation in the main TKE quantities downstream of a macro-roughness element located at $x = 4.32$ m is presented in figure 15. The accelerated class profiles are present near the top of the macro-roughness element; the S-shaped class profiles occur in the wake; and finally log class profiles occur in the more homogeneous bed topography region.

At the top of the element and slightly on the lee side, maximum TKE production occurs close to the bed. Maximum TKE production remains at this elevation downstream in the lee over the entire wake region, thus occurring higher off the local bed. This is line with DNS computations by Le *et al.* (1997, figures 24 and 25).

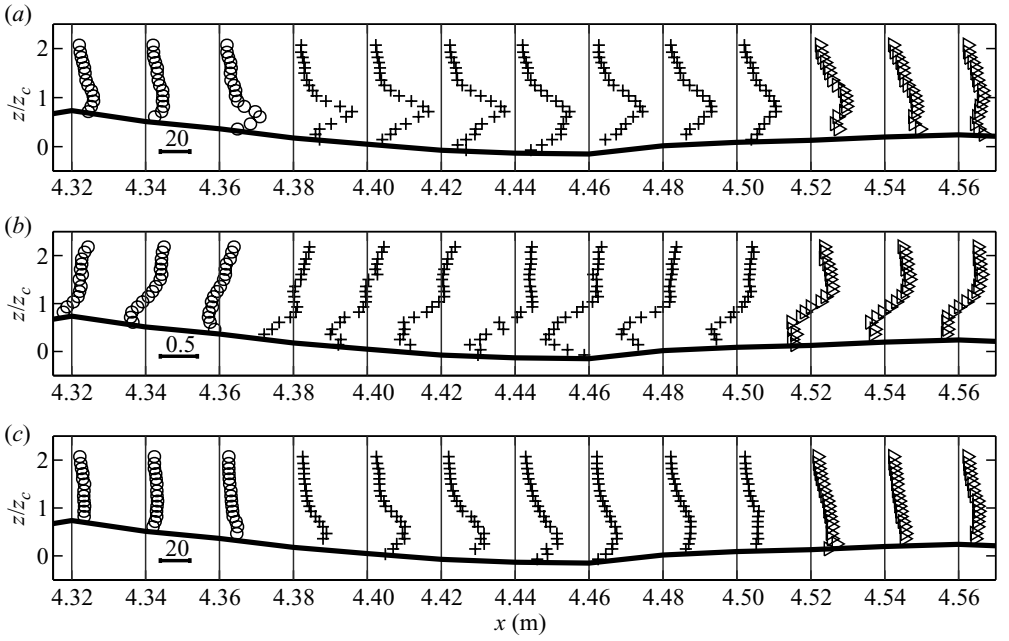

FIGURE 15. Profiles of TKE-related characteristics in the wake of a macro-roughness element. The solid line is the bottom elevation. Streamwise variation in (*a*) local TKE production Ph/u_*^3, (*b*) TKE flux F_k/u_*^3 and (*c*) turbulent dissipation $\epsilon h/u_{*s}^3$. For each profile the vertical line is the zero value. Symbols plotted on the left correspond to negative values. (▷): log; (+): S-shaped; (○): accelerated.

The researchers show that maximum TKE production remains at elevations close to $0.8D$ at least all the way to a downstream distance of seven times the step height (D). Extrapolation to our case using $D = z_c$ gives a downstream distance of 19 cm from the crest of the macro-roughness element, which closely fits with what can be observed in figure 15. The maximum vertically integrated TKE production occurs in the S-shaped profile area at section $x = 4.42$ m, that is midway in the wake. This is also similar to the computations by Le *et al.* (1997), which show that maximum TKE production seems to occur at a downstream distance of $4D$ which, for our case, would give roughly 11 cm. Further downstream, TKE production profiles tend to become more uniform, with less pronounced local maxima. Within the log class profiles in the downstream area, a small second TKE production maximum appears close to the bed and increases downstream, where it tends to reach the former higher maximum value (see figure 15*a*). It is interesting to note that in this portion of the domain, if double averaged the TKE production would reach its maximum at $z = 0.75\,z_c$. This explains why the double-averaged maximum TKE production of the whole section is located slightly below z_c and not at $z = z_c$ (figure 15*a*).

The spatial variation in F_k profiles is now analysed. At the top of the macro-roughness element F_k is approximately zero. However, in the lee side a strong negative F_k value near $z_c/2$ builds up (see figure 15*b*). The maximum negative F_k value occurs at $x = 4.46$ m, that is the location of the lowest bed elevation. Further downstream, the F_k profile tends to be more homogeneous, the maximum negative value decreasing until the entire profile resembles a typical log class F_k profile. Moreover, it should be noted that throughout the wake zone the $F_k = 0$ elevation remains relatively constant at $z = z_c$.

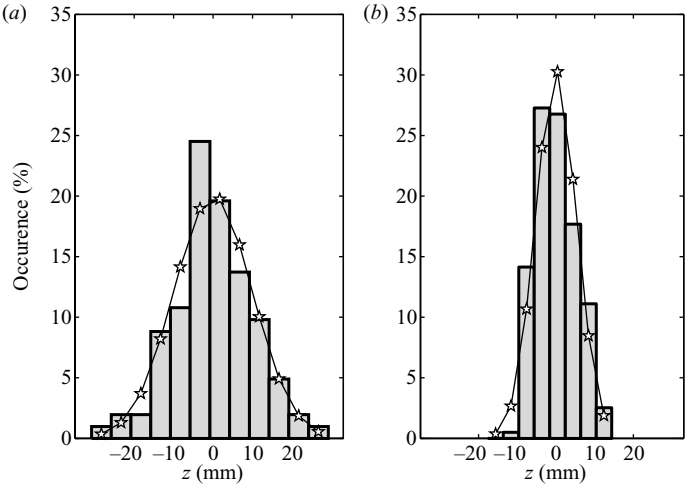

FIGURE 16. Bed elevation distribution for (*a*) Case 1 and (*b*) Case 2. (☆): equivalent gaussian function.

Finally, the variation in turbulent dissipation ϵ profile (see figure 15*c*) is fairly similar to that of P with a relatively homogeneous profile in the accelerated and log class areas and a strong increase in the S-shaped region at elevations around $z/z_c = 0.5$. Once again this behaviour has strong similarities with the computations by Le *et al.* (1997), which show that the maximum value of ϵ throughout the wake is slightly below that of the TKE production P and that its highest value is obtained at the same locations as P at a downstream distance of $4\,z_c \simeq 11$ cm.

The previously described variations in TKE quantities in a wake are very similar to those reported for a mixing layer and reattached mixing layers (Le *et al.* 1997). The initial velocity discontinuity is located at the top of the macro-roughness element, where flow separation occurs. The mean convective velocity is located slightly below z_c where the macro-roughness element turbulence mechanisms are of major importance (Pope 2003).

5.4. *Comparison with another statistical bed distribution*

Uniform flow over a man-made bed (Case 2) is now investigated. The gravel is forced into the bed so that the largest dimension of the gravel elements lies in the horizontal plane. This creates a different bed morphology that is useful for assessing whether the previous results can be generalized to cases in which the bed elevation distribution is narrower. Figure 16 compares the bed elevation distributions measured with the point gauge for the two cases investigated.

The distribution of bed elevations appears to be much narrower for Case 2. It is also noticeable that the distribution is quite symmetrical for Case 1, whereas it is slightly skewed for Case 2. These results are in qualitative agreement with observations made by Nikora, Goring & Biggs (1998) who found that the bed elevation distribution is symmetrical for unworked beds (like Case 1) but positively skewed for a worked bed (like Case 2). The measurement and data analysis methodology is exactly the same as that applied to Case 1 and described above. The flow characteristics are given in table 1. Concerning the local profile classification, the statistics of occurrence of the classes are modified with regard to the previous case. For Case 2, 31 profiles belong to the log class, 11 to the S-shaped class and only 3 to the accelerated class. The

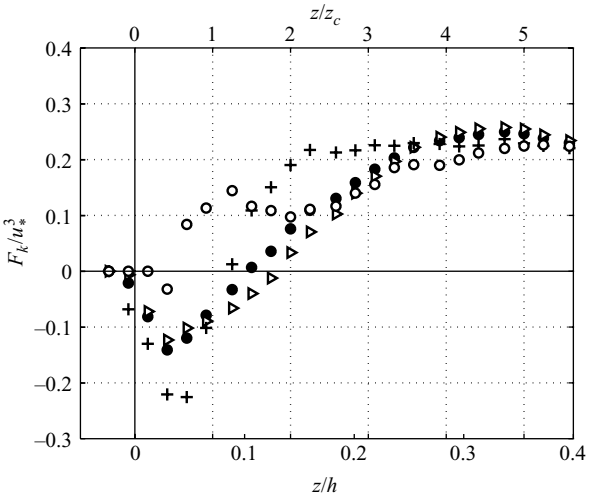

FIGURE 17. Case 2: superficial double-averaged TKE flux F_k profiles per class. (▷): log; (+): S-shaped; (○): accelerated; (●): all 45 profiles.

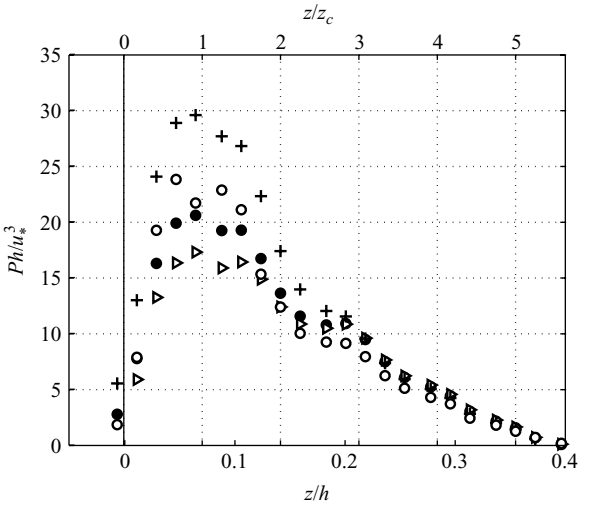

FIGURE 18. Case 2: Superficial double-averaged TKE production P profiles per class. (▷): log; (+): S-shaped; (○): accelerated; (●): all 45 profiles.

strong prevalence of the log class is a consequence of the narrower bed elevation distribution, leaving fewer and less pronounced macro-roughness elements.

Figures 17 and 18 present the profiles of F_k and TKE production P for Case 2 for each class and show that the global double-averaged TKE profiles are similar to those of Case 1. Concerning the turbulence flux term, it is noticeable that the minimum value in both cases occurs at $z/z_c \sim 0.5$. Secondly, the double-averaged log class profile of F_k reaches a maximum negative value of $-0.12\,u_*^3$ similar to Case 1, whereas the F_k of the S-shaped class reaches a maximum negative value of $-0.22\,u_*^3$, less pronounced than the $-0.34\,u_*^3$ value for the Case 1 (see figure 12). Consequently, in the second configuration, the 'weaker' S-shaped profiles lead to a less pronounced S-shaped class contribution and thus to a smaller maximum negative turbulent flux

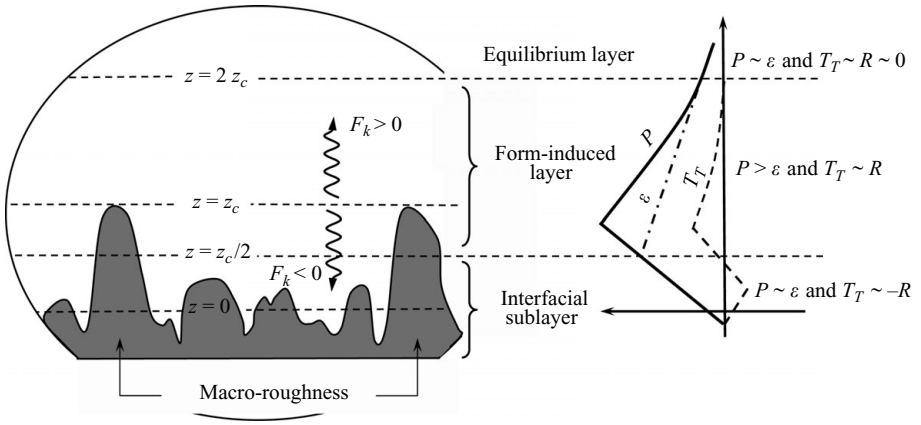

FIGURE 19. Schematic close-up of the bed/flow interface and the TKE budget.

for the overall double-averaged F_k profile at $z/z_c = 0.5$. Similarly, the S-shaped class maximum TKE production is reduced in Case 2 compared to Case 1. The maximum value for P in Case 1 occurs at $z/z_c \sim 0.8$, whereas in the Case 2 it occurs slightly higher at $z/z_c \sim 1$. This is probably due to the fact that, since the elevation distribution is narrower, the crests of all macro-roughness elements are all very close. Nonetheless, the maximum total double-averaged value of Ph/u_*^3 appears to be the same in both bed configurations (close to 21). The accelerated class contribution is the key factor in this balance. Indeed in Case 1 the accelerated class contains one fifth of all the verticals with a much smaller maximum class-averaged TKE production than in Case 2 which exhibits only one fifteenth of the verticals. Further investigation is required to confirm whether the maximum TKE production value is more or less universal for rough flows.

Consequently, the analysis of flow over the second bed topography (Case 2) does not qualitatively invalidate the overall picture of rough flows strongly influenced by mixing layers developing downstream of the crests of macro-roughness elements as in Case 1. The main difference for the averaged profiles per class is that the wake TKE production and diffusion are less energetic. It is suggested that this is related to the narrower bed elevation distribution with smaller troughs downstream of the macro-roughness elements, reducing the expansion of recirculations and thus producing less numerous and weaker profiles of the S-shaped type.

6. Discussion and conclusion

A schematic view of the TKE budget is given in figure 19 based on our experimental results. Our understanding is that above $2z_c$ TKE production nearly balances dissipation in a manner similar to that in the log-law region of smooth boundary layers. In this so-called equilibrium region, turbulent diffusion is generally found to be negligible.

In a layer between $2z_c$ and $z_c/2$, the TKE production term is larger than the dissipation term, and the turbulent diffusion term T_T is also maximum in this region. Turbulent diffusion actively diffuses the turbulence produced in the vicinity of $z = z_c$ in both directions: towards the bed ($F_k < 0$ for $z < z_c$) and towards the water surface ($F_k > 0$ for $z > z_c$) as in Raupach *et al.* (1991). This layer of high TKE production rates, exceeding dissipation by more than 80 %, can be called the form-induced layer,

since the macro-roughness elements create strong, detached mixing-type flows over the bed crest level.

Finally, towards the bed, F_k reaches a minimum value but still remains directed towards the bed. In the lower part of the roughness sub-layer, called interfacial sub-layer, the flow is characterized by a balance between a low dissipation and a low TKE production. Pressure diffusion (residue) is therefore the candidate to compensate for turbulent diffusion.

Above the roughness sublayer, for $z > z_c$, the streamwise velocity profiles and shear stress profiles strongly resemble those measured in uniform rough-bed flows with very high flow submergence (Nezu & Nakagawa 1993; Hurther & Lemmin 2000). The main difference lies in the fact that for large roughness flows, the maximum TKE production and turbulent diffusion values are located near z_c, far from the reference plane. This position corresponds to an elevation of $z^+ = 1500$. Moreover, the spatially averaged TKE budget characteristics are in good agreement with those obtained in flows over canopies (Raupach *et al.* 1991; Finnigan 2000; Lopez & Garcia 2001), at least up to about $3/2\, z_c$. This finding strongly supports the analogy with a mixing-layer-type flow, already mentioned for flows over canopies with a maximum shear plane located slightly below z_c, separating the high-velocity upper region from the smaller velocity lower roughness-interface region.

The local flow characterization revealed the presence of three classes of velocity profiles, called S-shaped, accelerated and log classes as proposed by Hoover & Ackerman (2004). The signature of each class on the different turbulent characteristics was analysed. It was shown that the local velocity profiles for the S-shaped class exhibit an inflectional trend typical of mixing layers. The profiles of the S-shape class were found to be located in the wakes downstream of the macro-roughness elements. Furthermore, it appears that these macro-roughness bed element wakes are of major importance in the turbulent kinetic energy budget, as they impose high magnitudes in the double-averaged shear, double-averaged TKE flux and dissipation. In particular, the double-averaged TKE production of the S-shaped class is twice as high as the total double-averaged TKE production. This highlights the importance of the hydrodynamics near the macro-roughness bed elements, since, even with very low occurrence (11 %), the superficial double-averaged maximum TKE production is increased by up to 30 % compared to typical logarithmic profiles. The question of whether the gravel beds can be characterized statistically in terms of class occurrence will have to be addressed in the future.

We are deeply indebted to Jean-Marc Barnoud, who renovated the LEGI flume, the Ecole Nationale Supérieure d'Hydraulique et de Mécanique de Grenoble, which provided funding for this rehabilitation in the framework of an engineering student project, and Mickaël Bricault for guidance in post-processing the acoustic intensity of the ADVP measurements. We are also grateful to the HYDRALAB III-SANDS project and CNRS-INSU programmes for their financial support.

REFERENCES

Aberle, J. 2007 Measurements of armour layer roughness geometry function and porosity. *Acta Geophys.* **55** (1), 23–32.

Antonia, R. A. & Krogstad, P.-A. 2001 Turbulence structure in boundary layers over different types of surface roughness. *Fluid Dyn. Res.* **28**, 139–157.

Balachandar, R. & Bhuiyan, F. 2007 Higher-order moments of velocity fluctuations in an open-channel flow with large bottom roughness. *J. Hydraul. Engng* **133** (1), 77–87.

Bigillon, F., Nino, Y. & Garcia, M. H. 2006 Measurements of turbulence characteristics in an open-channel flow over a transitionally-rough bed using particle image velocimetry. *Exp. Fluids* **41** (6), 857–867.

Blanckaert, K. & de Vriend, H. J. 2004 Secondary flow in sharp open-channel bends. *J. Fluid Mech.* **498**, 353–380.

Blanckaert, K. & de Vriend, H. J. 2005 Turbulence structure in sharp open-channel bends. *J. Fluid Mech.* **536**, 27–48.

Britter, R. E. & Hanna, S. R. 2003 Flow and dispersion in urban areas. *Ann. Rev. Fluid Mech.* **35**, 469–496.

Buffin-Belanger, T. & Roy, A. G. 1998 Effects of pebble cluster on the turbulent structure of a depth-limited flow in a gravel-bed river. *Geomorphology* **25**, 249–267.

Castro, I. T. 2007 Rough-wall boundary layers: mean flow universality. *J. Fluid Mech.* **585**, 469–485.

Chaudry, M. H. 1993 *Open-Channel Flow*. Prentice Hall.

Chow, V. T. 1959 *Open Channel Hydraulics*. McGraw-Hill.

Coceal, O., Dobre, A. & Belcher, S. E. 2007*a* Spatial variability of flow statistics within regular building arrays. *Boundary-Layer Meteorol.* **125**, 537–552.

Coceal, O., Dobre, A. & Thomas, T. G. 2007*b* Unsteady dynamics and organized structures from dns over an idealized building canopy. *Int. J. Climatol.* **27**, 1943–1953.

Coceal, O., Dobre, A., Thomas, T. G. & Belcher, S. E. 2007*c* Structure of turbulent flow over regular arrays of cubical roughness. *J. Fluid Mech.* **589**, 375–409.

Coceal, O., Thomas, T. G., Castro, I. P. & Belcher, S. E. 2006 Mean flow and turbulence statistics over groups of urban-like cubical obstacles. *Boundary-Layer Meteorol.* **121**, 491–519.

Coleman, S., Nikora, V., McLean, S., Clunie, T. & Melville, B. 2007 Subelement form-drag parameterization in rough-bed flows. *J. Hydraul. Engng* **133** (2), 121–129.

De Langres, E. 2008 Effects of wind on plants. *Ann. Rev. Fluid Mech.* **40**, 141–168.

Finnigan, J. 2000 Turbulence in plant canopies. *Ann. Rev. Fluid Mech.* **32**, 519–571.

Franca, M. J. 2005*a* A field study of turbulent flows in shallow gravel-bed rivers. PhD thesis no. 3393, Ecole Polytechnique Federale de Lausanne, Switzerland.

Franca, M. J. 2005*b* Flow dynamics over a gravel riverbed. In *Proc. of the XXXI IAHR Congress*, Seoul, Korea.

Franca, M. J. & Czernuszenko, W. 2006 Equivalent velocity profile for turbulent flows over gravel riverbeds. In *Proc. River Flow 2006*, Lisbon, Portugal.

Franca, M. J. & Lemmin, U. 2006 Turbulence measurements in shallow flows in gravel-bed rivers. In *Proceeding of the 7th ICHE*, Philadelphia, USA.

Garbini, J. L., Forster, F. K. & Jorgensen, J. E. 1982 Measurement of fluid turbulence based on pulsed ultrasound techniques. Part 1. Analysis. *J. Fluid Mech.* **118**, 445–470.

Graf, W. H. & Altinakar, M. 1998 *Fluvial Hydraulics: Flow and Transport Processes in Channels of Simple Geometry*. John Wiley.

Hoover, T. M. & Ackerman, J. D. 2004 Near-bed hydrodynamic measurements above boulders in shallow torrential streams: Implications for stream biota. *J. Environ. Engng. Sci.* **3**, 365–378.

Hurther, D. & Lemmin, U. 2000 Shear stress statistics and wall similarity analysis in turbulent boundary layers using a high-resolution 3-d ADVP. *J. Oceanic Engng* **25** (4), 446–457.

Hurther, D. & Lemmin, U. 2001 A correction method for turbulence measurements with a 3d acoustic doppler velocity profiler. *J. Atmos. Oceanic Technol.* **18** (3), 446–458.

Hurther, D. & Lemmin, U. 2003 Turbulent particle flux and momentum flux statistics in suspension flow. *Water Resour. Res.* **39** (5) 1139, doi:10.1029/2001WR001113.

Hurther, D. & Lemmin, U. 2008 Improved turbulence profiling with field adapted acoustic doppler velocimeters using a bi-frequency doppler noise suppression method. *J. Atmos. Oceanic Technol.* **25** (3), 452–463.

Hurther, D., Lemmin, U. & Terray, E. A. 2007 Turbulent transport in the outer region of rough wall open-channel flows: the contribution of large coherent shear stress structures (lc3s). *J. Fluid Mech.* **574**, 465–493.

Le, H., Moin, P. & Kim, J. 1997 Direct numerical simulation of turbulent flow over a backward-facing step. *J. Fluid Mech.* **330**, 349–374.

Lopez, F. & Garcia, M. H. 1999 Wall similarity in turbulent open channel flow. *J. Engng Mech.* **125**, 789–796.

Lopez, F. & Garcia, M. H. 2001 Mean flow and turbulence structure of open-channel flow through non-emergent vegetation. *J. Hydraul. Engng* **127** (5), 392–402.

Manes, C., Pokrajac, D. & McEwan, I. 2007 Double-averaged open-channel flows with small relative submergence. *J. Hydraul. Engng* **133** (8), 896–904.

Mignot, E., Barthélemy, E. & Hurther, D. 2008 Turbulent kinetic energy budget in a gravel-bed channel flow. *Acta Geophys.* **56** (3), 601–613.

Millikan, C. B. 1938 A critical discussion of turbulent flows in channels and circular pipes. In *Proc. of 5th Intl Conf. on Applied Mechanics*, New York.

Nakagawa, H. & Nezu, I. 1977 Prediction of the contribution to reynolds stress from bursting events in open-channel flows. *J. Fluid Mech.* **80** (1), 99–128.

Nakagawa, H., Nezu, I. & Ueda, H. 1975 Turbulence of open channel flow over smooth and rough beds. *Proc. Jpn. Soc. Civ. Eng.* **241**, 155–168.

Nelson, J. M., McLean, S. R. & Wolfe, S. R. 1993 Mean flow and turbulence fields over two-dimensional bed forms. *Water Resour. Res.* **29** (12), 3935–3953.

Nepf, H. & Ghisalberti, M. 2008 Flow and transport in channels with submerged vegetation. *Acta Geophys.* **56**, 753–777.

Nezu, I. 1993 Open-channel flow turbulence and its research prospect in the 21st century. *J. Hydraul. Engng.* **131** (4), 229–246.

Nezu, I. & Nakagawa, H. 1993 *Turbulence in open channel flows*. IAHR Monograph, Balkema, Rotterdam, The Netherlands.

Nikora, V., Goring, D. & Biggs, B. 1998 On gravel-bed roughness characterization. *Water Resour. Res.* **34** (3), 517–527.

Nikora, V., Goring, D., McEwan, I. & Griffiths, G. 2001 Spatially averaged open-channel flow over rough bed. *J. Hydraul. Engng* **127** (2), 123–133.

Nikora, V., Koll, K., McEwan, I., McLean, S. & Dittrich, I. A. 2004 Velocity distribution in the roughness layer of rough-bed flows. *J. Hydraulic Engng* **130** (10), 1036–1042.

Nikora, V., McEwan, I., S., McLean, Coleman, S., Pokrajac, D. & Walters, R. 2007 Double-averaging concept for rough-bed open-channel and overland flows: theoretical background. *J. Hydraul. Engng* **133** (8), 873–883.

Pope, S. B. 2003 *Turbulent Flows*. Cambridge University Press.

Raupach, M. R., Antonia, R. A. & Rajagopalan, S. 1981 Conditional statistics of reynolds stress in rough wall and smooth wall turbulent boundary layers. *J. Fluid Mech.* **108**, 363–382.

Raupach, M. R., Antonia, R. A. & Rajagopalan, S. 1991 Rough-wall turbulent boundary layers. *Appl. Mech. Rev.* **44** (1), 1–25.

Raupach, M. R., Finnigan, J. J. & Brunet, Y. 1996 Coherent eddies and turbulence in vegetation canopies: the mixing layer analogy. *Boundary-Layer Meteorol.* **78**, 351–382.

Raupach, M. R. & Shaw, R. H. 1982 Averaging procedures for flow within vegetation canopies. *Boundary-Layer Meteorol.* **22**, 79–90.

Serafin, R. & Lhermitte, R. 1984 Pulse-to-pulse coherent doppler sonar signal processing techniques. *J. Atmos. Oceanic Technol.* **1** (4), 293–308.

Shen, C. & Lemmin, U. 1997 Ultrasonic scattering in highly turbulent clear water flow. *Ultrasonics* **35**, 57–64.

Song, T., Graf, W. H. & Lemmin, U. 1994 Uniform flow in open channels with movable gravel bed. *J. Hydraul. Res.* **32** (6), 861–876.

Wilson, N. R. & Shaw, R. H. 1977 A higher order closure model for canopy flow. *J. Appl. Meteorol.* **16**, 1197–1205.